PCCP

Protobranching as Repulsion-Induced Attraction: A Prototype for Geminal Stabilization

Journal:	*Physical Chemistry Chemical Physics*
Manuscript ID	CP-ART-04-2020-002193.R3
Article Type:	Paper
Date Submitted by the Author:	09-Jul-2020
Complete List of Authors:	Joyce, Justin P.; Colorado State University, Chemistry Shores, Matthew; Colorado State University Rappe, Anthony; Colorado State University

ARTICLE

Protobranching as Repulsion-Induced Attraction: A Prototype for Geminal Stabilization

Received 00th January 20xx,
Accepted 00th January 20xx

DOI: 10.1039/x0xx00000x

Justin P. Joyce,[a] Matthew P. Shores [a] and Anthony K. Rappè *[a]

Noncovalent interactions are traditionally defined within the context of their attractive components, such as electrostatics and dispersion. Sources of molecular strain are derived through the destabilization of Coulombic and exchange repulsion. Due to this binary designation, the underlying origin of geminal stability with respect to alkanes (referred to as protobranching) has been an active subject for debate between these competing perspectives. We recast this stabilization as a complementary (*Gestalt*) interaction between dispersion and exchange repulsion, each impacting the other. We use triplet hydrogen and argon dimer as foundational van der Waals adducts to develop a procedure for the visualization and quantification of both exchange repulsion, $\Delta\rho_{SCF}$, and medium-range correlation, $\Delta\Delta\rho$, as perturbations in electron density. We use the framework of the DFT-D3 correction to reproduce the shape of the dispersion potential at medium range and successfully model the trend in stability for the eighteen isomers of octane with a diverse series of functionals: BLYP, B3LYP, BP86, PBE, and PBE0. Collectively, our findings show that protobranching is a manifestation of steric repulsion-reduction in vibrational enthalpy *and* medium-range electron correlation.

Introduction

Geminal (1,3) interactions are a fertile but under-explored source of energetic differentiation: They occur in all molecules larger than nuclear diatomic, their number increasing with chemical complexity. While these contacts are traditionally treated as afterthoughts to orbital hybridization at the central atom and electron pair repulsion,[1] geminal relationships are important in understanding the preferential stabilization of branched alkanes compared to their straight-chain isomers, a phenomenon known as protobranching (Figure 1).[2] These interactions are pivotal for comparing the thermodynamics of reaction pathways for the pyrolysis of hydrocarbons,[3,4] where low temperature, controlled pyrolosis is essential to improved isomeric product distribution in petroleum refinement and the viability of the emerging chemical recycling of olefin-based polymers.[5–7]

The physical origin of protobranching has been a source of passionate contention extending over sixty years. Conflicting reports by Pitzer and Catalano[8] and Bartell[9] initially assigned the 2 kcal mol^{-1} stability of *iso*-butane to attractive dispersion and nonbonded repulsion, respectively. These seemingly trivial systems have humbled traditional computational approaches. The speed and efficiency of DFT methods were challenged in the early part of the 21st century by their inability to treat hydrocarbons of greater complexity than butane, with errors approximately proportional to system size.[10–13] Previously attributed to reduced steric repulsion[14–18] and enhanced hyperconjugation[19–22], more recent reports propose that protobranching arises from medium-range correlation.[23–26] The decisive contribution of medium-range correlation for hydrocarbons was originally identified by Grimme and suggested as a critical benchmark system for functional development.[27]

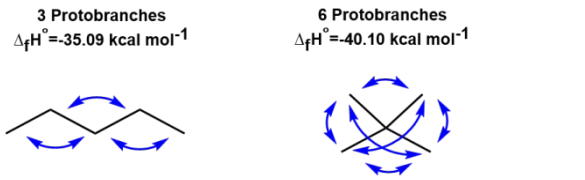

Figure 1. The $\Delta_f H°$ of *n*-pentane (left) and isopentane (right) where the blue arrows denote an alkyl-alkyl geminal contact, aka protobranch.

Pairwise medium-range electron correlation interactions occur at intermediate distances between a covalent bond distance and a nonbond contact. While dispersion is the omnipresent source of attraction, it is often associated with its long-range properties, which are defined by London's attractive dipole-dipole model. Exchange repulsion is a prerequisite for stability and the counterbalance to attractive electrostatics and dispersion. With few exceptions, researchers have overlooked its ability to facilitate noncovalent interactions.[28–31] Recent reports have highlighted exchange repulsion and dispersion as an "either-or" relationship where the two are in competition for molecular stability.[32–34] We note that exchange and Pauli repulsion are synonymous, and that it is always a constituent of steric repulsion, while electrostatics are system-dependent.

Here, we build upon these interpretations and present these seemingly opposing interactions as complementary: We argue their *interplay* is the source of protobranching. We frame this as a *Gestalt* interaction, in reference to the psychological school

[a] *Department of Chemistry, Colorado State University, Fort Collins, CO 80523, USA. E-mail: Anthony.Rappe@colostate.edu*

of thought, to illustrate their complementary nature despite their contrasting properties.

We begin by examining computed potential curves for a series of diatomic complexes. The medium-range properties of $^3H_2$ establish dispersion as a direct consequence of exchange repulsion. The attractive impact persists at separations on the order of a covalent bond. The canonical noble gas dimer, Ar_2, is used to develop a procedure for visualizing and quantifying the observation that exchange repulsion and dispersion are complementary perturbations of electron density. This contributes to recently developed methods to plot dispersion.[35–37] Next, we reparametrize the DFT-D3 dispersion correction, based on argon dimer, to reproduce medium-range dispersion.[38] We present our D3($^3Ar_2$) and D3(Ar_2) corrections as a treatment for medium-range correlation, as it reproduces protobranching within the eighteen isomers of octane when paired with a diverse set of popular DFT functionals. Collectively, our findings highlight the decisive contribution of dispersion as a natural consequence of exchange repulsion.

Results and Discussion

Dispersion Within the Repulsive Wall of Diatomic Species

The London model accurately describes the long-range attraction of dispersion, but its character within the repulsive wall is ambiguous.[36,39] These conditions are produced in scattering experiments of noble gases, where persistent stabilization at contracted separations has been observed.[40] Electron correlation at close contacts is inseparable from repulsion because overlapping electron densities violate the Pauli principle, a caveat London originally addressed.[41,42] We note that electron correlation predominantly consists of parallel and anti-parallel double excitations, which we refer to as triplet and singlet correlation, respectively. Dispersion has been largely attributed to triplet correlation.[43,44]

Triplet hydrogen, $^3H_2$, was selected as a model system as its electronic structure prohibits covalent bonding and allows for close approach.[45] A Full-CI calculation was performed on $^3H_2$ with an extended basis set and report an equilibrium separation of 4.15 Å that is stabilized by 0.013 kcal mol^{-1}, as presented in Figure 2.[46] The correlation energy (parallel excitations) was plotted alongside the London approximation, $C_6\ R^{-6}$. While the dipole-dipole model accounts for dispersion at extended separations, it deviates upon contraction due to its asymptotic decay. Dispersion persists as an attractive force far inside the van der Waals minimum, since triplet correlation displays a minimum at 0.70 Å, the approximate bond length of ground state H_2. It is noted that its maximal attraction of -3.6 kcal mol^{-1} is modest in comparison to the strength of the ground state H_2 covalent bond. Analogous curves were found for ^{2}HHe, $^1He_2$, and $^9C_2$ that are collected in Figures S1-S3.

When the H-H distance is shortened and their orbitals overlap, exchange repulsion destabilizes the ground state while the more diffuse excited state orbitals are stabilized due to interatomic potential attraction. Cumulatively, this lowers the excitation energy of the complex and increases the magnitude of electron correlation. Far from vanishing within the repulsive wall, exchange repulsion magnifies the contribution of dispersion. This interplay is depicted in Figure 3, which illustrates how the double excitations polarize their adjacent orbitals to yield the anticipated dipole-dipole attractions. Pitzer presented a similar interpretation of $^3H_2$ as a natural precursor to protobranching, although he was self-admittingly hindered by the computational capability of the period.[47]

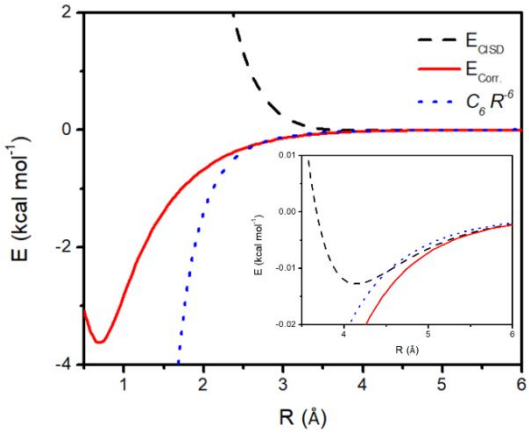

Figure 2. The Full-CI energy of $^3H_2$ (dashed black line) as a function of distance. The solid red line is the associated correlation energy while the dotted blue line presents the atom-pairwise dipole-dipole term (C_6 = -89.0 kcal mol^{-1} Å^6). The equilibrium separation is highlighted in the inset.

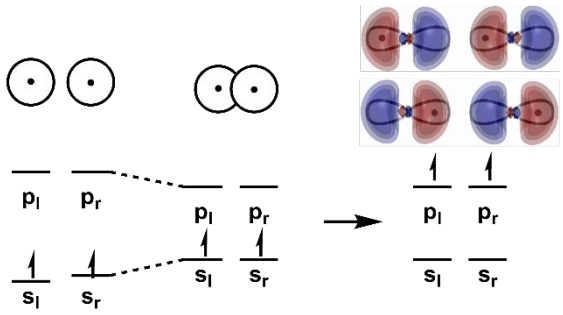

Figure 3. The perturbation of the ground and excited state of $^3H_2$ upon orbital overlap, where the black dots denote an electron. The parallel excitations of σ-symmetry are overlaid with their equivalent dipole-dipole attractions, where red and blue denote an excess and depletion of electron density, respectively.

We further characterized the interplay between exchange repulsion and electron correlation with respect to the noble gas dimer Ar_2, which has served as the basis for numerous dispersion corrections.[48–50] Figure 4 and Equation 1. detail the computed difference between the SCF electron density of Ar_2 and the isolated atoms. Bader and Ponder previously applied this formalism to exchange repulsion, which they analysed in terms of an electrostatic interaction, while Ruedenberg presented this as a quantum mechanical expression of kinetic energy.[29,51,52] This approach has been similarly extended to a study of the stabilizing forces in the metal-ligand bonding of Au(I) complexes.[53,54]

$$\Delta\rho_{SCF} = \rho_{Ar_2} - \rho_l - \rho_r \qquad \textbf{(1)}$$

Figure 4. presents the depletion of electron density from the area of overlap (*green*) and its subsequent localization on the respective fragments (*blue*). We attribute this to the orthogonalization of occupied orbitals. The DLPNO-CCSD(T) based Local Energy Decomposition (LED) method was used to calculate exchange repulsion as a function of distance, their separation (R ΣvdW^{-1}) scaled with respect to the sum of their van der Waals radii. This quantity is denoted as electronic preparation energy, $\Delta E_{HF}^{el-prep}$, in its original notation.[55] The *depleted*(-) electron density was summed within the area of overlap ($\Delta\rho_{SCF}^{-}$) and a strong exponential relationship with its corresponding value for exchange repulsion was found. Its units are percent of the density of a single electron and highlight that its magnitude never exceeds more than a fraction of an electron.

DLPNO-CCSD explicitly treats the double excitations that define dispersion. The impact of electron correlation was isolated by referencing its relative electron density to the associated SCF value as detailed in Equation 2. provided below:

$$\Delta\Delta\rho = \Delta\rho_{DLPNO-CCSD} - \Delta\rho_{SCF} \qquad (2)$$

The ΔΔρ plots in Figure 5. show a build-up of electron density in the area that is vacated through exchange repulsion. Electron correlation decreases exchange repulsion by permitting electron density to flow back into the overlap region. Rather than stabilization rooted in attractive polarization, the plots suggest that medium-range dispersion operates through a reduction in exchange repulsion. The summation of this electronic density build-up ($\Delta\Delta\rho^{+}$) follows an exponential relationship with respect to the LED assignment of dispersion. Further decomposition of the dispersion term denotes a nearly constant 3:1 contribution of parallel and anti-parallel excitations, respectively. The complementary relationship between exchange repulsion and dispersion is further validated through the strong exponential relationship between their LED terms and our $\Delta\rho_{SCF}^{-}$ and $\Delta\Delta\rho^{+}$ parameters, as included in Figure S6.

Fluctuations in electron density can be modulated with the existing framework of Spin-Component Scaled MP2 (SCS-MP2), that adjust the contributions of singlet and triplet correlation.[56] We varied these scaling factors for Ar_2 at a fixed distance and found that these terms display an identical impact on $\Delta\Delta\rho^{+}$, as presented in Figure S7. Unmodified MP2 exagerates the perturbation of correlated electron density. This agrees with its tendency to overestimate van der Waals adducts.[57,58] When the correlation energy is analyzed, its overestimation is due solely to intermolecular parallel excitations. The scaling factors previously published by Grimme (Singlet = $\frac{5}{4}$ and Triplet = $\frac{1}{3}$) largely correct for this and provide quantitative agreement with DLPNO-CCSD. This procedure could similarly be applied to double-hybrid DFT functionals.

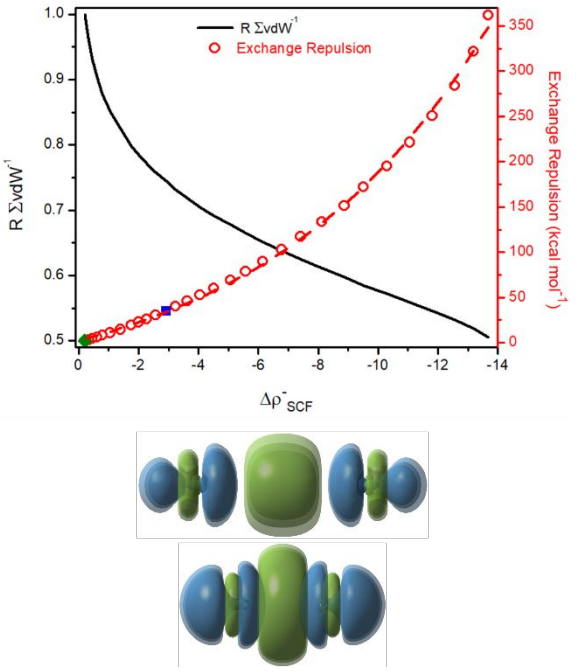

Figure 4. (Top) The variation of distance (black) and exchange repulsion (red) with respect to its $\Delta\rho_{SCF}^{-}$ value for Ar_2. The green diamond and blue square denote the Δρ plots presented in the middle (1.00 R ΣvdW^{-1}: 3.75 Å) and bottom panel (0.75 R ΣvdW^{-1} : 2.80 Å) , respectively. The contour of the $\Delta\rho_{SCF}$ plots are layered with isovalues of 4.00, 3.00, and 2.00 E^{-5} a.u., where the colors blue and green denote an increase and decrease in electron density, respectively.

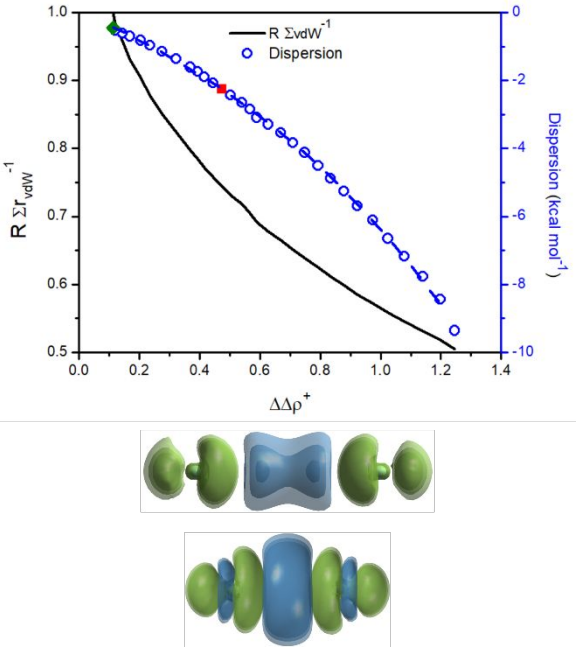

Figure 5. (Top) The variation of distance (black) and exchange repulsion (red) with respect to its $\Delta\Delta\rho^{+}$ value for Ar_2. The Green diamond and blue square denote the ΔΔρ plots presented in the middle (1.00 R ΣvdW^{-1}: 3.75 Å) and bottom panels (0.75 R ΣvdW^{-1} :2.80 Å), respectively. The contour of the ΔΔρ plots are layered with isovalues of 4.00, 3.00, and 2.00 E^{-5} where the colors blue and green denote an increase and decrease in electron density, respectively.

Application to Protobranching

The stabilization of geminal contacts reiterates the importance of dispersion within the repulsive wall, as we have detailed in the context of Ar_2. While we have shown that medium-range correlation can be modulated with SCS-MP2, this procedure quickly becomes cost-prohibitive with increasing size of the system. It is due to this expense that dispersion is routinely treated with the DFT-D3 correction, its formulation presented below.[38] Here, medium-range correlation is modelled with the expansion of the usual dipole-dipole (C_6) term to include its dipole-quadrupole (C_8) interactions. Due to the R^{-8} distance dependence of the dipole-quadrupole term it has a more pronounced contribution at close contacts. The DFT-D3 model corrects for the short-range, asymptotic, behaviour of the London approximation with a damping functional.[44,59,60]

While the a_1 and a_2 terms define the threshold distances within which dispersion is treated as a constant, the s_6 and s_8 parameters scale the contributions of dipole-dipole and dipole-quadrople interactions, respectively.

$$E_{disp}^{DFT\text{-}D3} = -\frac{1}{2}\sum_{A \neq Bn = 6,8}\sum \frac{s_n C_n^{AB}}{R^n + \left(a_1\sqrt{\frac{C_8^{AB}}{C_6^{AB}}} + a_2\right)^n} \qquad \textbf{(3)}$$

The inability of DFT to treat dispersion is traditionally associated with its long-range behaviour operating outside of the bounds of the local density approximation.[61,62] Dispersion corrections are often addressed with a pragmatic approach in order to avoid 'double counting' due to the ambiguous assignment of electron correlation by the exchange-correlation functional of DFT methods.[63] It has been reported that the D3 correction compounds error upon contraction from equilibrium separation.[64–66] We addressed this limitation with a reparameterization, DFT-D3M, through expansion of the benchmark set to more adequately weigh structures that have short-range non-bonded contacts.[67]

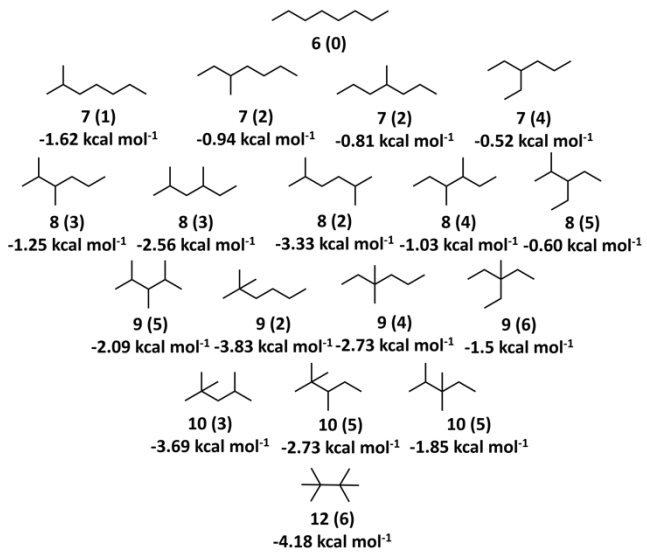

Figure 6. The eighteen structural isomers of octane. Their number of protobranches are included alongside their *gauche*-torsional modes, in parenthesis. Their experimental $\Delta\Delta_fH°$, with respect to *n*-octane, are included below.

The stabilization of 2,2,3,3-tetramethyl-butane with respect to *n*-octane has been employed as a benchmark for functional development due to the challenges associated with its treatment: The structures possess six to twelve protobranches, zero to six *gauche*-conformations and their stabilization ($\Delta\Delta_fH°$) ranges across 4 kcal mol^{-1}.[68–71] Geminal-alkyl, alkyl and *gauche*-contacts are separated by approximately 0.75 (2.55 Å) and 0.90 R ΣvdW^{-1} (3.06 Å), respectively. We expand upon this and consider the relative stability of the eighteen isomers of octane, as shown in Figure 6.

The experimental values for $\Delta\Delta_fH°$ do not account for variations in the zero-point energy and the temperature dependence of the enthalpy ($\Delta\Delta_{trv}H°$) and the thermal population of higher-energy torsional modes ($\Delta\Delta_{config.}H°$) to the absolute energy difference (ΔE), as detailed below. Gronert previously attributed hydrocarbon stability to the reduced steric interactions of alkane branching.[14] We find that approximately 15-30% of protobranch attraction derives from $\Delta\Delta_{trv}H°$. Figure 7. shows its inverse relationship to number of geminal contacts, where a negative value indicates weaker bond strength. We found a similar trend for gauche torsional modes, vicinal (1,4) contacts, that similarly increase with alkane branching. This suggests that geminal and vicinal contacts are a source of strain in paraffins that paradoxically contributes to protobranching stability.

$$\Delta\Delta_fH° = \Delta E + \Delta\Delta_{trv}H° + \Delta\Delta_{config.}H° \qquad \textbf{(4)}$$

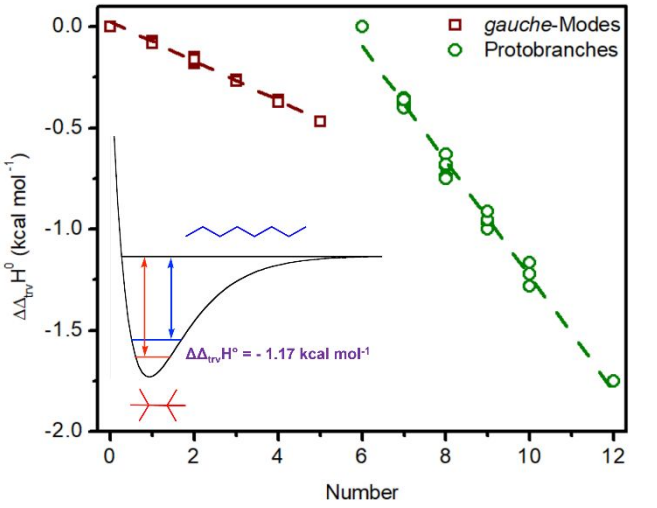

Figure 7. The relative enthalpy ($\Delta\Delta_{trv}H°$) with respect to the trans-conformation of *n*-octane. The open-brown squares denote the twenty-two *gauche*-conformations of *n*-octane. The open-navy circles present the number of protobranches for the eighteen isomers of octane, corrected for their number of *gauche*-conformations. Their linear fit is shown by the associated dashed line, as included in the ESI. The inset depicts the $\Delta\Delta_{trv}H°$ of 2,2,3,3-tetramethyl-butane (red) with respect to n-octane (blue).

Based on our characterization of repulsive diatomic species, these components of strain should concertedly enhance electron correlation. Figure 8. shows DLPNO-CCSD(T) calculates a -0.80 and -1.15 kcal mol^{-1} stabilization of the cumulative

singlet and triplet correlation ($\Delta E^{C\text{-}CCSD}$) for the *gauche*-torsional modes and geminal-alkyl, alkyl contacts of the octane series, respectively. The isodesmic reaction for the formation of propane from ethane and methane estimates its relative stability as -2.8 kcal mol^{-1} suggesting that approximately half of the protobranching phenomenon is due to medium-range correlation. In relation, MP2 overestimates their attractive nature and assigns a relative correlation stabilization, $\Delta E^{C\text{-}MP2}$, of -1.09 and -1.70 kcal mol^{-1} for vicinal and geminal contacts, respectively. The SCS-MP2 procedure largely corrects the MP2 error and reports $\Delta E^{C\text{-}MP2}$ of -0.81 and -1.40 kcal mol^{-1} for *gauche*-modes and protobranching, respectively. This agrees with our $\Delta\Delta\rho^{+}$ analysis of Ar_2 that suggests that SCS-MP2 reproduces the impact of medium-range correlation.

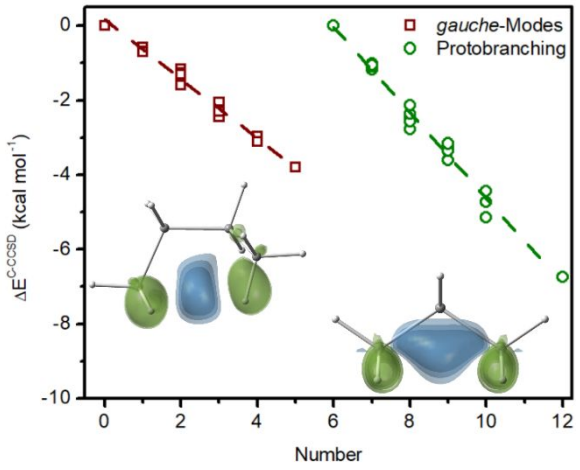

Figure 8. The relative parallel and anti-parallel correlation energy ($\Delta E^{C\text{-}CCSD}$) with respect to the *trans*-conformation of *n*-octane. The open-brown squares denote the twenty-two *gauche*-conformations of *n*-octane. The open-navy circles present the number of protobranches for the eighteen isomers of octane, corrected for their number of *gauche*-conformations. Their linear fit is shown by the associated dashed line, as included in the ESI. The inset depicts the $\Delta\Delta\rho$ plots the *gauche*-conformation of *n*-butane (left) and the protobranch of propane (right), its procedure detailed in the Experimental.

We used agreement between theoretical and experimental $\Delta\Delta_f H°$ for the eighteen isomers of octane as a measure of performance for a diverse series of functionals that have been previously parameterized for the DFT-D3 and D3M corrections: BLYP, B3LYP, BP86, PBE, and PBE0. In agreement with prior results, the unmodified functionals fail to model the $\Delta\Delta H°_f$ of extended alkanes.[29] While no linear trends are displayed, ($R^2 \approx 0$), the chosen functionals treat alkane branching as net repulsive, as shown in Figure S9. The functionals display a strong linear relationship between the error in the DFT functional with respect to experiment, ($\delta\Delta\Delta_f H°$), and $\Delta E^{C\text{-}CCSD}$ as shown in Figure 9. This relationship suggests these functionals do not address the stabilization associated with medium-range correlation. The challenges associated with obtaining a proper long-range exchange term have been discussed extensively in the literature.[72–76]

We build upon our findings to develop functional-independent dispersion corrections. We fit the s_8, a_1, and a_2 parameters of Equation 3. to the LED assignment of dispersion for Ar_2 to separations of up to 0.80 R ΣvdW^{-1}. We refer to this dispersion correction as D3(Ar_2). However, the exchange-hole dipole model of Becke and Johnson treats dispersion as the natural extension of exchange repulsion. Of similar interest, the LYP correlation functional is derived from electron correlation in the ground state of the helium atom and thus precludes triplet correlation. To address this, we further decomposed the LED dispersion term into its constituent triplet correlation to generate the data for the fit for a D3($^3Ar_2$) correction. For Ar2, triplet and singlet correlation possess an approximate 3:1 ratio that decays with decreased separation. We anticipate that DFT functionals whose slope of $\delta\Delta\Delta_f H(\Delta E^{C\text{-}CCSD})$ are roughly 1.0 and 0.75 will be most compatible with the D3(Ar_2) and D3($^3Ar_2$) correction, respectively. Both methods can be implemented within the current versions of the Gaussian and ORCA electronic structure software packages, their syntax included in the ESI.

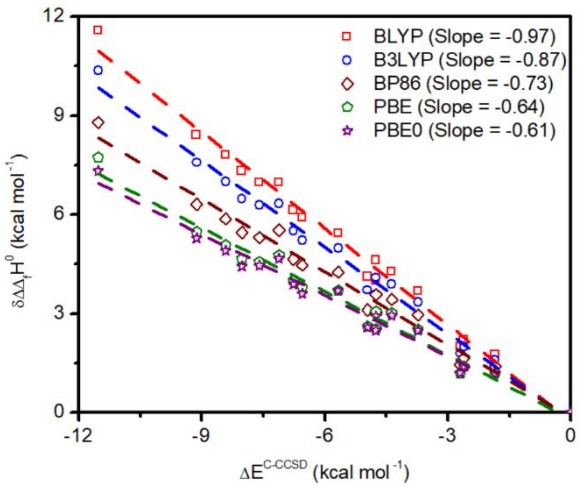

Figure 9. The relationship between the error of the detailed DFT functional, with respect to the experimental $\Delta\Delta H°$ ($\delta\Delta\Delta_f H°$) , and $\Delta E^{C\text{-}CCSD}$. BLYP (red squares), B3LYP (blue circles), BP86 (brown diamonds), PBE (green pentagon), and PBE0 (purple stars) are reported alongside their slope.

We first consider the D3, D3M, D3($^3Ar_2$), and D3(Ar_2) dispersion corrections for the popular B3LYP and PBE0 hybrid-DFT functionals, shown in Figure 10. The D3 correction dramatically improves both functionals for the isomeric energies of octane, although it consistently underestimates geminal stabilization and is weakly correlated with experiment. Performance is modestly improved with use of the D3M correction which also addresses medium-range correlation, albeit through a different parameterization procedure than ours. The strongest performance is obtained with the D3($^3Ar_2$) and D3(Ar_2) corrections for PBE0 and B3LYP, respectively.

The performance of the selected functionals in tandem with their D3 and D3M corrections, as well as the current D3($^3Ar_2$) and D3(Ar_2) corrections, are collected in Table 1. and shown in Figures S10-14. While BLYP and B3LYP are best paired with D3(Ar_2), the BP86, PBE, and PBE0 functionals are closer aligned with D3($^3Ar_2$). These results are consistent with their $\delta\Delta\Delta_f H(\Delta E^{C\text{-}CCSD})$ dependence. In no instance do the DFT-D3 or D3M corrections outperform the current Ar_2 based scheme. We emphasize that the parameters of the current corrections are

not optimized for any discrete functionals. A wavefunction-based conceptualization of electron correlation is compatible with DFT, whose functionals require a dispersion correction.

	DFT	-D3	-D3M	-D3($^3Ar_2$)	-D3(Ar_2)
BLYP	0.255 (0.018)	0.549 (0.500)	0.690 (0.772)	0.764 0.802)	**0.823 (0.872)**
B3LYP	-0.334 (0.041)	0.543 (0.483)	0.648 (0.688)	0.753 (0.821)	**0.990 (0.955)**
BP86	0.029 (0.000)	0.680 (0.811)	0.688 (0.833)	**0.937 (0.927)**	1.133 (0.893)
PBE	0.154 (0.016)	0.559 (0.508)	0.645 (0.689)	**1.036 (0.937)**	1.264 (0.837)
PBE0	0.154 (0.016)	0.575 (0.536)	0.677 (0.729)	**1.113 (0.911)**	1.343 (0.799)

Table 1. The slope (and R^2) of the linear best-fit between $\Delta\Delta_fH°$, calculated with the specified DFT functional and dispersion correction, and their experimental values. The dispersion correction that resulted in the closest agreement to experiment in bolded in red. The full equation of each fit, including their y-intercept, can be found in the ESI.

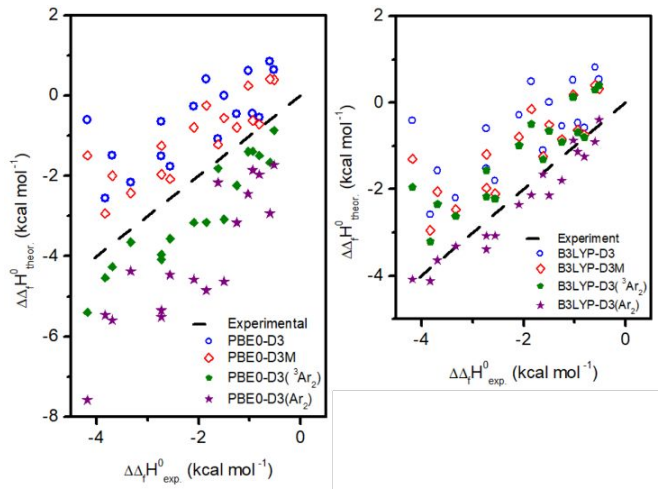

Figure 10. The relationship between $\Delta\Delta_fH°$ calculated with the PBE0 (left) and B3LYP (right) DFT functionals with respect to experiment. Each functional is used with their DFT-D3 (blue circles) and D3M (red diamonds) corrections and our D3($^3Ar_2$) (green pentagon) and D3(Ar_2) (purple stars) parameters.

Lastly, we detail the performance of a series of modern functionals: APF-D, ωB97X-D, ωB97X-D3, M06-2X, MN15, and DSD-BLYP-D3. APF-D and ωB97X-D significantly underestimate the stability of alkane branching while ωB97X-D3 and MN15 exaggerate its impact. As shown in Figure S15., medium-range correlation remains a challenge for modern DFT functionals. M06-2X reproduces the relative enthalpies of the octane series, noting that alkane isomerization energetics was included in its parameterization.[70] The double-hybrid DSD-BLYP-D3 functional accurately assigns the stability of the octane series, in agreement with previous benchmark studies.[77] It is particularly noteworthy that the APF functional, a 41.1, 58.9% combination of B3PW91 and PBE0, parameters selected to minimize spurious interactions in the Ne dimer displays quantitative accuracy (Slope = 1.00, R^2 = 0.955) when paired with the current D3($^3Ar_2$) correction.

Conclusion

Foundational van der Waals adducts were used to observe the persistence of dispersion at separations on the order of a covalent bond. This is a consequence of exchange repulsion. A quantitative procedure is developed that permits visualization of exchange repulsion ($\Delta\rho_{SCF}$) and medium-range correlation ($\Delta\Delta\rho$) as complementary perturbations in electron density. Classified as a *Gestalt* interaction, the interplay between medium-range correlation and steric repulsion resolves conflicting reports in the literatue of the origin of the protobranching. The framework of the DFT-D3 correction is used to reproduce the medium-range dispersion of Ar_2 and its constituent triplet correlation that yields the reported D3(Ar_2) and D3($^3Ar_2$) corrections, respectively. With the application of either of the corrections to a diverse series of popular DFT functionals the $\Delta\Delta H°_f$ for the octane series are accurately reproduced. Depending on perspective, one could see protobranching as the result of either attraction or repulsion. But to fully characterize the scope of the interaction, one must acknowledge the interplay between the seemingly paradoxical pairing.

Experimental

The following calculations were performed with the Gaussian09 electronic structure software package.[78] The $^3H_2$ potential energy curve used a CISD wavefunction[79], its basis set and polarization functionals developed from the references provided.[46,80] The $^9C_2$ surface was generated with a CCSD(T)[81,82] wavefunction using an aug-cc-pvtz[83–86] basis augmented by d (0.86, 0.436, 0.219, 0.11), f(0.86, 0.308, 0.12), g(0.36, 0.14), and h(0.17) polarization functions. The analogous ^{2}HHe and $^1He_2$ calculations were performed with Gaussian16[87] at the CCSD(T) level of theory with an aug-cc-pV5Z basis set. The basis set superposition error (BSSE) was addressed with a counterpoise correction.[88]

Computations for Ar_2 were performed with the ORCA 4.1 electronic structure software package[89] with the aug-cc-pVQZ basis set and its associated auxiliary basis set, within RIJK approach[90,91]. The reported geometries were calculated at the restricted Hartree-Fock and DLPNO-CCSD level of theory. The DLPNO-CCSD(T)[92,93] based Local Energy Decomposition (LED)[94] module was conducted with TightSCF and TightPNO[95,96] criteria. MP2[97] and SCS-MP2[56] were performed with an unrestricted wavefunction and the RI-approximation with the basis set previously described. The contribution of Singlet (E_S) and Triplet (E_T) correlation were calculated with the following equations:[43]

$$E_T = \frac{3}{2}(E_{\alpha\alpha} + E_{\beta\beta})$$

$$E_S = E_{\alpha\beta} - \frac{1}{3}E_T$$

The $\Delta\rho^{SCF}$ and $\Delta\Delta\rho$ plots were generated through subtraction of the specified electron density in the context of Gaussian cubes. The DLPNO-CCSD and MP2 electron densities

applied were unrelaxed and relaxed, respectively. The $\Delta\rho^{-}_{SCF}$ and $\Delta\Delta\rho^{+}$ values were calculated through separately integrating the positive and negative electron densities for the area of overlap. As previously detailed, the ΔΔρ plots of the geminal and vicinal contact of propane and *n*-butane in Figure 8,, respectively, were generated by replacing their methyl groups with BH_3.[98]

The DFT-D3($^3Ar_2$) correction has the following parameters:
s_6 = 1.0000, s_8 = 0.35050, a_1 = 0.06010, a_2 = 4.63455

The DFT-D3(Ar_2) correction has the following parameters:
s_6 = 1.0000, s_8 = 0.99838, a_1 = 0.11019, a_2 = 4.64540

For the octane series, vibrational frequencies and zero point correction were calculated using the APF hybrid density functional[99] with our D3($^3Ar_2$) dispersion correction and a def2-TZVP basis set.[100] The $\Delta\Delta_{config.}H°$ was taken as a Boltzmann distribution of the individual conformations as an ideal gas at 298 K enthalpies and referenced against *n*-octane. Both variables were applied as constants for the specified functionals. The eighteen isomers of octane were optimized at the detailed level-of-theory with the specified dispersion correction and a def2-TZVP basis set. The BLYP[101], B3LYP[102], BP86[103,104], PBE[105], PBE0[106], APF[99], ωB97X-D[107], M06-2X[108], and MN15[109] functionals were calculated using Gaussian16. An analogous procedure was used in ORCA 4.1 for the optimization of the ωB97X-D3[110], MP2[97], SCS-MP2[56], and DSD-BLYP-D3[38,111] functionals. The RI-approximation was used for the MP2 methods. DLPNO-CCSD(T) was calculated with an aug-cc-pVTZ, and its associated auxiliary, basis set and TightPNO settings with the SCS-MP2 optimized geometries. Functional performance was determined by experimental values from the National Institute of Standards and Technology (NIST).[112]

Conflicts of interest

There are no conflicts to declare.

Acknowledgements

This research was carried out by the Catalysis Collaboratory for Light-activated Earth Abundant Reagents (C-CLEAR), which is supported by the National Science Foundation (NSF) and the Environmental Protection Agency through the Networks for Sustainable Molecular Design and Synthesis (CHE-1339674). Computational efforts utilized the RMACC Summit supercomputer, which is supported by NSF (ACI-1532235 and ACI-1532236), Colorado State University, and the University of Colorado, Boulder. We also thank NSF for support of MPS and JPJ (CHE-1800554).

Notes and references

1 R. J. Gillespie, *Coord. Chem. Rev.*, 2008, 252, 1315–1327.
2 M. D. Wodrich, C. S. Wannere, Y. Mo, P. D. Jarowski, K. N. Houk and P. von R. Schleyer, *Chem. Eur. J.*, 2007, **13**, 7731–7744.
3 D. A. Leathard and J. H. Purnell, *Annu. Rev. Phys. Chem.*, 1970, **21**, 197–224.
4 E. E. Ba, S. Karahan, Z. Köstereli, M. Haktan and V. Aviyente, *J. Phys. Chem. A*, 2020, 0–28.
5 X. Jing, H. Wen, X. Gong, Z. Xu and A. Kajetanowicz, *Fuel Process. Technol.*, 2020, **201**, 106346.
6 L. Cheng, J. Gu, Y. Wang, J. Zhang, H. Yuan and Y. Chen, *Chem. Eng. J.*, 2020, **385**, 123866.
7 Y. Guan, J. Lou, R. Liu, H. Ma and J. Song, *Fuel*, 2020, **261**, 116447.
8 K. S. Pitzer and E. Catalano, *J. Am. Chem. Soc.*, 1956, **78**, 4844–4846.
9 L. S. Bartell, *J. Chem. Phys.*, 1960, **32**, 827–831.
10 P. C. Redfern, P. Zapol, L. A. Curtiss and K. Raghavachari, *J. Phys. Chem. A*, 2000, **104**, 5850–5854.
11 L. A. Curtiss, K. Raghavachari, P. C. Redfern and J. A. Pople, *J. Chem. Phys.*, 2000, **112**, 7374–7383.
12 M. D. Wodrich, C. Corminboeuf and P. von R. Schleyer, *Org. Lett.*, 2006, **8**, 3631–3634.
13 P. R. Schreiner, A. A. Fokin, R. A. Pascal, and A. de Meijere, *Org. Lett.*, 2006, **8**, 3635–3638.
14 S. Gronert, *J. Org. Chem.*, 2006, **71**, 1209–1219.
15 S. Gronert, *Chem. Eur. J.*, 2009, **15**, 5372–5382.
16 S. Gronert, *Chem. Eur. J.*, 2013, **19**, 11090–11092.
17 C. Rüchardt and H.-D. Beckhaus, *Angew. Chemie Int. Ed. English*, 1980, **19**, 429–440.
18 C. Rüchardt and H.-D. Beckhaus, *Angew. Chemie Int. Ed. English*, 1985, **24**, 529–538.
19 M. J. S. Dewar, *J. Am. Chem. Soc.*, 1984, **106**, 669–682.
20 J. Ma and S. Inagaki, *J. Am. Chem. Soc.*, 2001, **123**, 1193–1198.
21 C. R. Kemnitz, J. L. Mackey, M. J. Loewen, J. L. Hargrove, J. L. Lewis, W. E. Hawkins and A. F. Nielsen, *Chem. Eur. J.*, 2010, **16**, 6942–6949.
22 C. R. Kemnitz, *Chem. Eur. J.*, 2013, **19**, 11093–11095.
23 L. S. Bartell, *J. Phys. Chem. A*, 2012, **116**, 10460–10462.
24 W. C. McKee and P. von R. Schleyer, *J. Am. Chem. Soc.*, 2013, **135**, 13008–13014.
25 S. Grimme, *Org. Lett.*, 2010, **12**, 4670–4673.
26 R. M. Parrish, J. F. Gonthier, C. Corminbœuf and C. D. Sherrill, *J. Chem. Phys.*, 2015, **143**, 051103.
27 S. Grimme, *Angew. Chemie Int. Ed.*, 2006, **45**, 4460–4464.
28 A. J. Stone, *J. Am. Chem. Soc.*, 2013, **135**, 7005–7009.
29 J. A. Rackers and J. W. Ponder, *J. Chem. Phys.*, 2019, **150**, 084104.
30 P. Vermeeren, T. A. Hamlin, I. Fernández and F. M. Bickelhaupt, *Angew. Chemie*, 2020, **132**, 6260–6265.
31 K. Carter-Fenk and J. M. Herbert, *Chem. Sci.*, , DOI:10.1039/d0sc02667k.
32 S. E. Wheeler, T. J. Seguin, Y. Guan and A. C. Doney, *Acc. Chem. Res.*, 2016, **49**, 1061–1069.
33 S. Rösel, J. Becker, W. D. Allen and P. R. Schreiner, *J. Am. Chem. Soc.*, 2018, **140**, 14421–14432.
34 D. Yepes, F. Neese, B. List and G. Bistoni, *J. Am. Chem. Soc.*, 2020, **142**, 3613–3625.
35 J. Contreras-García, E. R. Johnson, S. Keinan, R. Chaudret, J. P. Piquemal, D. N. Beratan and W. Yang, *J. Chem. Theory Comput.*, 2011, **7**, 625–632.
36 A. Altun, F. Neese and G. Bistoni, *J. Chem. Theory Comput.*,

2019, **15**, 215–228.
37 R. Pollice and P. Chen, *Angew. Chemie Int. Ed.*, 2019, **58**, 9758–9769.
38 S. Grimme, S. Ehrlich and L. Goerigk, *J. Comput. Chem.*, 2011, **32**, 1456–1465.
39 S. Grimme, A. Hansen, J. G. Brandenburg and C. Bannwarth, *Chem. Rev.*, 2016, **116**, 5105–5154.
40 E. W. Rothe, L. L. Marino, R. H. Neynaber, P. K. Rol and S. M. Trujillo, *Phys. Rev.*, 1962, **126**, 598–602.
41 D. G. Truhlar, *J. Chem. Educ.*, 2019, **96**, 1671–1675.
42 F. London, *Trans. Faraday Soc.*, 1937, **33**, 8–26.
43 J. M. L. Martin, *J. Phys. Chem. A*, 2013, **117**, 3118–3132.
44 A. D. Becke and E. R. Johnson, *J. Chem. Phys.*, 2005, **123**, 154101.
45 R. Ahlrichs, R. Penco and G. Scoles, *Chem. Phys.*, 1977, **19**, 119–130.
46 E. Jakubikova, A. K. Rappé and E. R. Bernstein, *J. Phys. Chem. A*, 2006, **110**, 9529–9541.
47 W. E. Donath and K. S. Pitzer, *J. Am. Chem. Soc.*, 1956, **78**, 4562–4565.
48 R. Ahlrichs, R. Penco and G. Scoles, *Chem. Phys.*, 1977, **19**, 119–130.
49 R. A. Aziz and H. H. Chen, *J. Chem. Phys.*, 1977, **67**, 5719–5726.
50 A. Altun, F. Neese and G. Bistoni, *J. Chem. Theory Comput.*, 2019, **15**, 5894–5907.
51 R. F. W. Bader, *Chem. Eur. J.*, 2006, **12**, 2896–2901.
52 W. H. E. Schwarz, P. Valtazanos and K. Ruedenberg, *Theor. Chim. Acta*, 1985, **68**, 471–506.
53 G. Bistoni, L. Belpassi and F. Tarantelli, *Angew. Chemie - Int. Ed.*, 2013, **52**, 11599–11602.
54 G. Bistoni, S. Rampino, N. Scafuri, G. Ciancaleoni, D. Zuccaccia, L. Belpassi and F. Tarantelli, *Chem. Sci.*, 2016, **7**, 1174–1184.
55 W. B. Schneider, G. Bistoni, M. Sparta, M. Saitow, C. Riplinger, A. A. Auer and F. Neese, *J. Chem. Theory Comput.*, 2016, **12**, 4778–4792.
56 S. Grimme, *J. Chem. Phys.*, 2003, **118**, 9095–9102.
57 M. O. Sinnokrot, E. F. Valeev and C. D. Sherrill, *J. Am. Chem. Soc.*, 2002, **124**, 10887–10893.
58 S. Grimme, C. Mück-Lichtenfeld and J. Antony, *Phys. Chem. Chem. Phys.*, 2008, **10**, 3327–3334.
59 E. R. Johnson and A. D. Becke, *J. Chem. Phys.*, 2006, **124**, 174104.
60 A. D. Becke and E. R. Johnson, *J. Chem. Phys.*, 2007, **127**, 154108.
61 S. Kristyán and P. Pulay, *Chem. Phys. Lett.*, 1994, **229**, 175–180.
62 J. M. Pérez-Jordá and A. D. Becke, *Chem. Phys. Lett.*, 1995, **233**, 134–137.
63 S. Grimme, J. Antony, S. Ehrlich and H. Krieg, *J. Chem. Phys.*, 2010, **132**, 154104.
64 D. G. A. Smith and K. Patkowski, *J. Phys. Chem. C*, 2015, **119**, 4934–4948.
65 S. Li, D. G. A. Smith and K. Patkowski, *Phys. Chem. Chem. Phys.*, 2015, **17**, 16560–16574.
66 J. Witte, N. Mardirossian, J. B. Neaton and M. Head-Gordon, *J. Chem. Theory Comput.*, 2017, **13**, 2043–2052.
67 D. G. A. Smith, L. A. Burns, K. Patkowski and C. D. Sherrill, *J. Phys. Chem. Lett.*, 2016, **7**, 2197–2203.
68 S. Grimme, *J. Phys. Chem. A*, 2005, **109**, 3067–3077.
69 M. D. Wodrich, D. F. Jana, P. von R. Schleyer and C. Corminboeuf, *J. Phys. Chem. A*, 2008, **112**, 11495–11500.
70 Y. Zhao and D. G. Truhlar, *Org. Lett.*, 2006, **8**, 5753–5755.
71 P. R. Schreiner, *Angew. Chemie - Int. Ed.*, 2007, **46**, 4217–4219.
72 L. Gallandi, N. Marom, P. Rinke and T. Körzdörfer, *J. Chem. Theory Comput.*, 2016, **12**, 605–614.
73 M. J. Gillan, *J. Chem. Phys.*, 2014, **141**, 224106.
74 K. Pernal, R. Podeszwa, K. Patkowski and K. Szalewicz, *Phys. Rev. Lett.*, 2009, **103**, 1–4.
75 W. Zhang, Y.; Pan, W.; Yang, *J. Chem. Phys.*, 1997, 7921.
76 D. J. Lacks and R. G. Gordon, *Phys. Rev. A*, 1993, **47**, 4681–4690.
77 L. Goerigk, A. Hansen, C. Bauer, S. Ehrlich, A. Najibi and S. Grimme, *Phys. Chem. Chem. Phys.*, 2017, **19**, 32184–32215.
78 M. J. Frisch, G. W. Trucks, H. B. Schlegel, G. E. Scuseria, M. A. Robb, J. R. Cheeseman, G. Scalmani, V. Barone, G. A. Petersson, H. Nakatsuji, X. Li, M. Caricato, A. Marenich, J. Bloino, B. G. Janesko, R. Gomperts, B. Mennucci, H. P. Hratchian, J. V. Ortiz, A. F. Izmaylov, J. L. Sonnenberg, D. Williams-Young, F. Ding, F. Lipparini, F. Egidi, J. Goings, B. Peng, A. Petrone, T. Henderson, D. Ranasinghe, V. G. Zakrzewski, J. Gao, N. Rega, G. Zheng, W. Liang, M. Hada, M. Ehara, K. Toyota, R. Fukuda, J. Hasegawa, M. Ishida, T. Nakajima, Y. Honda, O. Kitao, H. Nakai, T. Vreven, K. Throssell, J. A. Montgomery, Jr., J. E. Peralta, F. Ogliaro, M. Bearpark, J. J. Heyd, E. Brothers, K. N. Kudin, V. N. Staroverov, T. Keith, R. Kobayashi, J. Normand, K. Raghavachari, A. Rendell, J. C. Burant, S. S. Iyengar, J. Tomasi, M. Cossi, J. M. Millam, M. Klene, C. Adamo, R. Cammi, J. W. Ochterski, R. L. Martin, K. Morokuma, O. Farkas, J. B. Foresman, and D. J. Fox Gaussian 9, Revision D.01; Gaussian, Inc.: Wallingford, CT, 2009.
79 J. A. Pople, R. Krishnan, H. B. Schlegel and J. S. Binkley, *Int. J. Quantum Chem.*, 2009, **16**, 225–241.
80 A. K. Rappé and E. R. Bernstein, *J. Phys. Chem. A*, 2000, **104**, 6117–6128.
81 G. D. Purvis and R. J. Bartlett, *J. Chem. Phys.*, 1982, **76**, 1910–1918.
82 J. A. Pople, M. Head-Gordon and K. Raghavachari, *J. Chem. Phys.*, 1987, **87**, 5968–5975.
83 D. E. Woon and T. H. Dunning, *J. Chem. Phys.*, 1995, **103**, 4572–4585.
84 K. A. Peterson and T. H. Dunning, *J. Chem. Phys.*, 2002, **117**, 10548–10560.
85 N. B. Balabanov and K. A. Peterson, *J. Chem. Phys.*, 2005, **123**, 064107.
86 T. H. Dunning, *J. Chem. Phys.*, 1989, **90**, 1007–1023.
87 Frisch, M. J.; Trucks, G. W.; Schlegel, H. B.; Scuseria, G. E.; Robb, M. A.; Cheeseman, J. R.; Scalmani, G.; Barone, V.; Petersson, G. A.; Nakatsuji, H.; Li, X.; Caricato, M.; Marenich, A. V.; Bloino, J.;Janesko, B. G.; Gomperts, R.; Mennucci, B.; Hratchian, H. P.; Ortiz, J.V.; Izmaylov, A. F.;

Sonnenberg, J. L.; Williams-Young, D.; Ding, F.; Lipparini, F.; Egidi, F.; Goings, J.; Peng, B.; Petrone, A.; Henderson, T.; Ranasinghe, D.; Zakrzewski, V. G.; Gao, J.; Rega, N.; Zheng, G.; Liang, W.; Hada, M.; Ehara, M.; Toyota, K.; Fukuda, R.; Hasegawa, J.; Ishida, M.; Nakajima, T.; Honda, Y.; Kitao, O.; Nakai, H.; Vreven, T.; Throssell, K.; Montgomery, J. A., Jr.; Peralta, J. E.; Ogliaro, F.; Bearpark, M. J.; Heyd, J. J.; Brothers, E. N.; Kudin, K. N.; Staroverov, V. N.; Keith, T. A.; Kobayashi, R.; Normand, J.; Raghavachari, K.; Rendell, A. P.; Burant, J. C.; Iyengar, S. S.; Tomasi, J.; Cossi, M.; Millam, J. M.; Klene, M.; Adamo, C.; Cammi, R.; Ochterski, J. W.; Martin, R. L.; Morokuma, K.; Farkas, O.; Foresman, J. B.; Fox, D. J. Gaussian 16, Revision A.03; Gaussian, Inc.: Wallingford, CT, 2016.

88 S. F. Boys and F. Bernardi, *Mol. Phys.*, 1970, **19**, 553–566.

89 F. Neese, *WIREs Comput. Mol. Sci.*, , DOI:10.1002/wcms.1327.

90 F. Weigend, M. Häser, H. Patzelt and R. Ahlrichs, *Chem. Phys. Lett.*, 1998, **294**, 143–152.

91 K. Eichkorn, O. Treutler, H. Öhm, M. Häser and R. Ahlrichs, *Chem. Phys. Lett.*, 1995, **240**, 283–290.

92 C. Riplinger and F. Neese, *J. Chem. Phys.*, 2013, **138**, 034106.

93 M. Saitow, U. Becker, C. Riplinger, E. F. Valeev and F. Neese, *J. Chem. Phys.*, 2017, **146**, 164105.

94 W. B. Schneider, G. Bistoni, M. Sparta, M. Saitow, C. Riplinger, A. A. Auer and F. Neese, *J. Chem. Theory Comput.*, 2016, **12**, 4778–4792.

95 C. Riplinger, P. Pinski, U. Becker, E. F. Valeev and F. Neese, *J. Chem. Phys.*, 2016, **144**, 024109.

96 D. G. Liakos, M. Sparta, M. K. Kesharwani, J. M. L. Martin and F. Neese, *J. Chem. Theory Comput.*, 2015, **11**, 1525–1539.

97 C. Møller and M. S. Plesset, *Phys. Rev.*, 1934, **46**, 618–622.

98 S. Gronert, *J. Org. Chem.*, 2006, **71**, 7045–7048.

99 A. Austin, G. A. Petersson, M. J. Frisch, F. J. Dobek, G. Scalmani and K. Throssell, *J. Chem. Theory Comput.*, 2012, **8**, 4989–5007.

100 F. Weigend and R. Ahlrichs, *Phys. Chem. Chem. Phys.*, 2005, **7**, 3297–3305.

101 B. Miehlich, A. Savin, H. Stoll and H. Preuss, *Chem. Phys. Lett.*, 1989, **157**, 200–206.

102 A. D. Becke, *J. Chem. Phys*, 1993, **98**, 5648.

103 A. D. Becke, *Phys. Rev. A*, 1988, **38**, 3098–3100.

104 J. P. Perdew, *Phys. Rev. B*, 1986, **33**, 8822–8824.

105 J. P. Perdew, K. Burke and M. Ernzerhof, *Phys. Rev. Lett.*, 1996, **77**, 3865–3868.

106 C. Adamo and V. Barone, *J. Chem. Phys.*, 1999, **110**, 6158–6170.

107 J. Da Chai and M. Head-Gordon, *Phys. Chem. Chem. Phys.*, 2008, **10**, 6615–6620.

108 Y. Zhao and D. G. Truhlar, *Theor. Chem. Acc.*, 2008, **120**, 215–241.

109 H. S. Yu, X. He, S. L. Li and D. G. Truhlar, *Chem. Sci.*, 2016, **7**, 5032–5051.

110 A. Najibi and L. Goerigk, *J. Chem. Theory Comput.*, 2018, **14**, 5725–5738.

111 S. Kozuch, D. Gruzman and J. M. L. Martin, *J. Phys. Chem. C*, 2010, **114**, 20801–20808.

112 NIST Standard Reference Database, https://webbook.nist.gov/chemistry/.

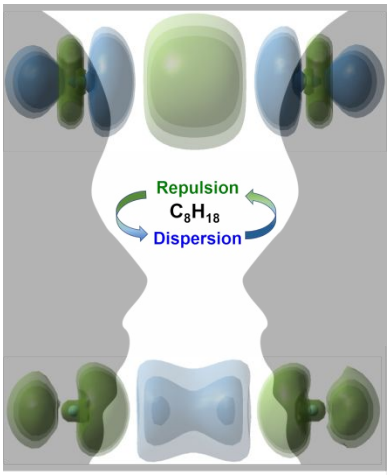

The complementarity of overlap-induced exhange repulsion and electron correlative dispersion suggests that each is important to a complete understanding of branched hydrocarbon stability.